



This is a repository copy of *Coassembled nanostructured bioscaffold reduces the expression of proinflammatory cytokines to induce apoptosis in epithelial cancer cells.*

White Rose Research Online URL for this paper:  
<http://eprints.whiterose.ac.uk/100798/>

Version: Accepted Version

---

**Article:**

Li, R., Pavuluri, S., Bruggeman, K. et al. (10 more authors) (2016) Coassembled nanostructured bioscaffold reduces the expression of proinflammatory cytokines to induce apoptosis in epithelial cancer cells. *Nanomedicine: Nanotechnology, Biology and Medicine*, 12 (5). pp. 1397-1407. ISSN 1549-9634

<https://doi.org/10.1016/j.nano.2016.01.009>

---

Article available under the terms of the CC-BY-NC-ND licence  
(<https://creativecommons.org/licenses/by-nc-nd/4.0/>)

**Reuse**

This article is distributed under the terms of the Creative Commons Attribution-NonCommercial-NoDerivs (CC BY-NC-ND) licence. This licence only allows you to download this work and share it with others as long as you credit the authors, but you can't change the article in any way or use it commercially. More information and the full terms of the licence here: <https://creativecommons.org/licenses/>

**Takedown**

If you consider content in White Rose Research Online to be in breach of UK law, please notify us by emailing [eprints@whiterose.ac.uk](mailto:eprints@whiterose.ac.uk) including the URL of the record and the reason for the withdrawal request.

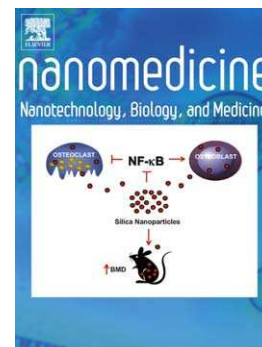


[eprints@whiterose.ac.uk](mailto:eprints@whiterose.ac.uk)  
<https://eprints.whiterose.ac.uk/>

## Accepted Manuscript

Coassembled nanostructured bioscaffold reduces the expression of proinflammatory cytokines to induce apoptosis in epithelial cancer cells

Rui Li, Sivapriya Pavuluri, Kiara Bruggeman, Benjamin M. Long, Andrew J. Parnell, Anne Martel, Steven R. Parnell, Frederick M. Pfeffer, Andrew J.C. Dennison, Kevin R. Nicholas, Colin J. Barrow, David R. Nisbet, Richard J. Williams



PII: S1549-9634(16)00079-4  
DOI: doi: [10.1016/j.nano.2016.01.009](https://doi.org/10.1016/j.nano.2016.01.009)  
Reference: NANO 1278

To appear in: *Nanomedicine: Nanotechnology, Biology, and Medicine*

Received date: 29 September 2015  
Revised date: 11 January 2016  
Accepted date: 21 January 2016

Please cite this article as: Li Rui, Pavuluri Sivapriya, Bruggeman Kiara, Long Benjamin M., Parnell Andrew J., Martel Anne, Parnell Steven R., Pfeffer Frederick M., Dennison Andrew J.C., Nicholas Kevin R., Barrow Colin J., Nisbet David R., Williams Richard J., Coassembled nanostructured bioscaffold reduces the expression of proinflammatory cytokines to induce apoptosis in epithelial cancer cells, *Nanomedicine: Nanotechnology, Biology, and Medicine* (2016), doi: [10.1016/j.nano.2016.01.009](https://doi.org/10.1016/j.nano.2016.01.009)

This is a PDF file of an unedited manuscript that has been accepted for publication. As a service to our customers we are providing this early version of the manuscript. The manuscript will undergo copyediting, typesetting, and review of the resulting proof before it is published in its final form. Please note that during the production process errors may be discovered which could affect the content, and all legal disclaimers that apply to the journal pertain.

## **Coassembled nanostructured bioscaffold reduces the expression of proinflammatory cytokines to induce apoptosis in epithelial cancer cells**

*Rui Li<sup>1,6</sup>, Sivapriya Pavuluri<sup>1,7</sup>, Kiara Bruggeman<sup>2</sup>, Benjamin M. Long<sup>1</sup>, Andrew J. Parnell<sup>3</sup>, , Anne Martel<sup>4</sup>, Steven R. Parnell<sup>5</sup>, Frederick M. Pfeiffer<sup>1</sup>, Andrew J.C. Dennison<sup>4</sup>, Kevin R. Nicholas<sup>1,7</sup>, Colin J. Barrow<sup>1</sup>, David R. Nisbet<sup>2a</sup> and Richard J. Williams<sup>1,8a\*</sup>*

1. Centre for Chemistry and Biotechnology, Deakin University, Waurn Ponds, Australia.
  2. Research School of Engineering, The Australian National University, Canberra, Australia,
  3. Department of Physics and Astronomy, University of Sheffield, United Kingdom
  - 4 Institut Laue Langevin, Grenoble, France
  - 5 Low Energy Neutron Source (LENS) Indiana University, Bloomington, Indiana, U.S.A
  6. Coconut Research Institute of Chinese Academy of Tropical Agricultural Sciences, Wenchang 571339, Hainan, China
  7. School of Medicine, Deakin University, Waurn Ponds, VIC, Australia
  - 8.School of Aerospace, Mechanical and Manufacturing Engineering and the Health Innovations Research Institute, RMIT University, Melbourne, Australia.
- a. DRN and RJW contributed equally to this work

\*To whom correspondence should be addressed. Email: Richard.Williams@RMIT.edu.au

Abstract Word count: 149

Total body text and figure caption word Count: 4985

Number of figures: 5 main text, 1 supplemental.

Number of references: 49

The local inflammatory environment of the cell promotes the growth of epithelial cancers. Therefore, controlling inflammation locally using a material in a sustained, non-steroidal fashion can effectively kill malignant cells without significant damage to surrounding healthy cells. A promising class of materials for such applications are the nanostructured scaffolds formed by epitope containing minimalist self-assembled peptides (SAPs), as they are bioactive on a cellular length scale, whilst presenting as an easily handled hydrogel. Here, we show that the assembly process distributes an anti-inflammatory polysaccharide, fuccoidan, localised to the nanofibers to function as an anti-inflammatory biomaterial for cancer therapy. We show that it supports healthy cells, whilst inducing apoptosis in cancerous endothelial cells, as demonstrated by the downregulation of the proinflammatory gene and protein expression pathways associated with epithelial cancer progression. Our findings highlight an innovative material approach with potential applications as local epithelial cancer immunotherapy and drug delivery vehicles.

## Background

The use of designed, nanostructured materials for the treatment of cancers is a rapidly growing research area<sup>1</sup> as they can potentially mimic the tumour microenvironment<sup>2</sup>. A promising approach involves materials that can mediate the local tumour environment through attenuation of the inflammatory response<sup>3</sup>, whilst simultaneously providing a stable healthy extracellular matrix (ECM) mimic to promote regeneration<sup>4</sup>. The link between the inflammatory response and the promotion of cancers is well established; notably in endothelial cancers such as oral, pancreatic and colon<sup>5</sup>. Epidemiological studies have shown that chronic inflammation is a significant causative factor for these cancers; several studies showed promising anti-tumorigenic effects using non-steroidal anti-inflammatory drugs<sup>6</sup>. Hence, a therapeutic opportunity lies in developing a biocompatible material that can achieve a spatially confined, sustained, non-steroidal and selective suppression of the immune system<sup>7</sup>. A range of cancer therapies could benefit from this approach; such a material could provide an anti-tumoral void-filling support for the surrounding healthy tissue following surgical excision, or, alternatively, a topical treatment for the surface of a lesion<sup>8</sup>. Numerous examples exist of complex hierarchical ECM assemblies, formed by the self-organisation of a range of cellularly-secreted small molecules, that provide structure and function in living systems<sup>9</sup>. In particular, polysaccharides and fibrous proteins assemble to form networks that support multicellular systems and mediate cellular interactions with their surrounding microenvironment<sup>10</sup>. A family of sulfonated polysaccharides known as fucoidans have gathered increasing attention for their inherent biocompatibility and anti-inflammatory properties both *in vitro* and *in vivo*<sup>11</sup>. Importantly, several studies have also indicated the anti-mitogenic effects of fucoidans as they block cell cycle progression<sup>12</sup>, induce apoptosis and reduce tumorigenicity in several cancer cell lines<sup>13</sup>. However, the use of these biopolymers as a therapeutic is constrained by the high solubility of the polysaccharide chains, limiting their sustained functionality unless encapsulated in an external carrier<sup>14</sup> or presented on a two-

dimensional (2D) surface<sup>15</sup>. The motivation for this work, therefore, was to present constrained fucoidan on the surface of a three dimensional (3D) ECM-like scaffold.

Hydrogels formed by bioinspired synthetic organic molecules known as self-assembling peptides (SAP) are highly suitable materials for cancer therapy<sup>16</sup>, as they have been shown to form nanofibrillar matrices of similar morphology<sup>17</sup> which are functional both *in vitro*<sup>18</sup> and *in vivo*<sup>19</sup> through the inclusion of bioactive and biocompatible peptide sequences in the SAP during synthesis<sup>20</sup>. The formation of SAP hydrogels is a thermodynamically driven process<sup>21</sup>; control over the organisation of the structures formed is achieved through careful exploitation of assembly conditions, such as manipulation of the molecule's specific pKa<sup>22</sup>, biocatalysis<sup>21</sup> or the rate of assembly<sup>23</sup>. Such facile control over the final structures means they are excellent candidates for use as tailored multicomponent adjuvant scaffolds. Key to such applications, SAPs have been shown to have multicomponent functionality, as the noncovalent forces that govern their assembly can be used to physically incorporate larger molecules such as proteins<sup>24</sup> or drugs<sup>25</sup> making them an ideal candidate material for the immobilisation and functional presentation of the otherwise highly soluble fucoidan polysaccharides as part of a self-assembled matrix.

## Methods

See supplementary information for full synthetic and analytical procedures.

*Co-Assembled Hydrogel Formation:* 10.0 mg of Fmoc-FRGDF along with mixtures of 2 mg fucoidan (Marinova Pty Ltd, Cambridge, Tasmanian, Australia) were added to separate 4 mL glass vials. 400  $\mu$ L Milli-Q water (purified by Milli-Q Advantage A10 System, Merck Milipore, Australia) was added into each vial, then pH increased by the addition of a minimal volume of 0.5 M NaOH while vortexing and then neutralised to pH 7.4 via dropwise addition

of 0.1 M HCl (Asia Pacific Specialty Chemicals Ltd., Australia). Finally, 100 mM PBS (pH 7.4) was added into the solution to bring the total volume up to 1.0 mL, and used 48 hours later

*NMR Studies:* 2.5 mg of Fmoc-FRGDF was added to a glass vial and dissolved in 0.5 mL of D<sub>2</sub>O. The pH was increased using freshly prepared 0.5 M NaOD (NaOH in D<sub>2</sub>O) and vortexed until a transparent solution was obtained. The resulting solution was transferred to a 5 mm NMR tube. <sup>1</sup>H, COSY, HMBC and HSQC spectra were collected on a Bruker AVANCE III 500 MHz FT-NMR spectrometer. <sup>13</sup>C resonances were elucidated using both Heteronuclear Multiple-Bond Correlation spectroscopy (HMBC) and Heteronuclear Single-Quantum Correlation spectroscopy (HSQC)

*Small-Angle Neutron Scattering (SANS):* SANS measurements were performed on the D33 instrument at the Institut Laue-Langevin, Grenoble, France<sup>26</sup> in fixed wavelength mode using a wavelength of 6Å and a wavelength resolution of  $\Delta\lambda=10\%$  at detector distances of 2m and 12m to cover the  $Q$ -range 0.001-0.5Å<sup>-1</sup>. Data collected for the two detector distances were joined using the GRAS<sub>ans</sub>P package, reduced using the NIST SANS reduction macros<sup>27</sup> and the resultant SANS curves fit using the SASview package. A flexible cylinder model was used to fit the data. The data for fmoc-FRGDF was fit using constraints on the scattering lengths of the buffer and peptide. Kratky analysis was performed using the NIST SANS analysis macros<sup>27</sup>. Contrast matching to fucoidan was performed by measuring SANS from a series of 10 mg/mL fucoidan solutions in H<sub>2</sub>O/D<sub>2</sub>O mixtures. SANS from the chosen concentration of 21.5% confirmed that there was no detectable scattering from the fucoidan solution. Peptide samples were measured in sealed 1mm path-length Hellma cells.

*Cell lines and culture conditions:* The human tongue squamous cell carcinoma cell line (SCC25) cultures were obtained verified from ATCC and were maintained in DMEM-F12 complete medium containing 10% fetal bovine serum, 400 ng/mL hydrocortisone and penicillin/streptomycin. The human mammary fibroblast cell line (hMFC) cultures were maintained as described previously<sup>18a</sup>. Cell line cultures were maintained at 37°C with 5% CO<sub>2</sub>.

*Reverse Transcription and Quantitative PCR:* Total RNA was reverse-transcribed to generate complimentary DNA using Superscript III (Invitrogen) following the manufacturer's protocol. To challenge fucoidan, cells were stimulated with LPS (sigma) at a concentration of 10 µg/mL in the complete media. Differential expression of the genes examined was listed in supplementary Table 1. 30 ng of cDNA was used to perform quantitative real time PCR in a 20 µL reaction using SYBR Green (Biorad) on a CFX connect<sup>TM</sup> Real Time PCR detection system (Biorad). Primer oligosequences were designed using Primer3 PCR prime design tool (Whitehead Institute for Biomedical Research, Cambridge, MA, USA) and the gene specificity was checked using National Center for Biotechnology Information nucleotide database. Steps followed during QPCR to generate amplification curves include an initial denaturing step for 3 min at 95°C, followed by 40 cycles of 95°C for 10 s, 60°C for 30 s and 72°C for 30 s. The expression of each gene in terms of fold change was normalised to the housekeeping gene ACTB.

*NF-κB and CEP55 staining:* SCC25 cells treated without and with fucoidan (2 mg/mL) for 48 h. Cells were fixed with paraformaldehyde and permeabilised with 0.1% triton-x-100. Cells were blocked with 1% bovine serum albumin (BSA) in PBS for 1 h at room temperature and further treated with primary antibody (Rabbit polyclonal NFκB p65 antibody and Rabbit monoclonal CEP55 antibody, abcam) overnight at 4°C. Cells were further incubated with

anti-rabbit alexa fluor 488 secondary conjugates for 1 h at room temperature. Following several washes cells were visualised under fluorescence microscope (Nikon).

*Annexin V staining* SCC25 cells treated without and with fucoidan (2 mg/mL) for 48 h were stained with the Alexa Fluor® 488 annexin V/Dead Cell Apoptosis Kit (life technologies) Cells were also counter stained with Hoechst dye to stain the live cells. Images were obtained through fluorescence microscopy (Nikon Eclipse Ti-S)

## Results

*The formation of two-component hydrogels and evaluation of (i) their biocompatibility and (ii) their effect on cancer cells.*

In order to form the scaffold to present fucoidan, we used a biocompatible minimalist pentapeptide sequence known to assemble via a  $\pi$ - $\beta$  self-assembly mechanism, fluorenylmethoxycarbonyl (Fmoc) FRGDF (Figure 1)<sup>17-18</sup>. Fmoc-FRGDF was synthesised using a standard solid phase Fmoc peptide synthesis methodology to yield a white crystalline powder (see electronic supplementary information). Fucoidan was supplied in a readily solubilised powder of similar consistency. We mixed both powders together and initiated self-assembly using a well-established pH switch methodology<sup>18a, 22</sup>. The solution was then made up to a final concentration of 10 mg/mL Fmoc-FRGDF and 2 mg/mL fucoidan with Dulbeccos' Modified Eagle Medium (DMEM), and the hydrogel was allowed to form. When this was compared to a pure Fmoc-FRGDF hydrogel, both formed optically clear, stable hydrogels (Supplementary Figure 1a).

Biocompatibility of the systems was measured with 3D cell cultures of human mammary fibroblast cells as a control for healthy tissue, and the moderately differentiated oral tongue squamous cell carcinoma line SCC25<sup>28</sup>. Cell viability of hMFC on the hydrogels of Fmoc-

FRGDF (0RGD) and hydrogels co-assembled with 2 mg/mL of fucoidan (2RGD) was determined using an MTS assay up to 72 hours with no significant difference, whereas SCC25 cells showed a reduction in the number of viable cells (Figure 2a). A live/dead cell assay performed at 48 hours (to observe cell death mid-cycle) showed significant numbers of dead SCC25 cells, evenly distributed throughout the material (Figure 2b). To observe which cells were apoptotic, SCC25 cells were cultured for 48 hours prior to staining with Annexin V, propidium iodide and Hoechst stain to observe cell death mid-cycle (Figure 2c,d).

#### *Analysis of the two component self-assembly*

Four samples were prepared: 1) **Fmoc-FRGDF**: a hydrogel formed by the pH triggered assembly at a concentration of 10 mg/mL; 2) **Co-Assembly**: whereby 10 mg/mL Fmoc-FRGDF and 2 mg/mL fucoidan were mixed in powdered form prior to application of a pH switch; 3) **Post-Assembly**: a preformed Fmoc-FRGDF hydrogel with a solution of fucoidan added 12 hours post-assembly by mixing to the same final concentration as 2); and 4) **Fucoidan**: 2 mg/mL solution of fucoidan. As expected, samples 1-3 formed self-supporting hydrogels, whereas 4 remained a solution.

We visualised the structures formed in each sample with transmission electron microscopy (TEM) to determine the underlying nanostructures and atomic force microscopy (AFM) to evaluate the microstructure of the system (Figure 3). Fourier transform infra-red spectroscopy (FTIR) to confirm that the peptide-like organisation was not disrupted. This confirmed that the addition of fucoidan during the assembly process did not affect the molecular packing of the peptides into the anti-parallel  $\beta$ -sheets which drive these assemblies and result in peaks at  $\sim 1630\text{ cm}^{-1}$  and  $\sim 1690\text{ cm}^{-1}$  (Figure 3i)<sup>29</sup>. We then analysed the chiral organisation of the structures within the samples using circular dichroism (CD)<sup>22, 24a, 30</sup>. Characteristic and retained transitions were observed in the region between 230-280 nm. The mechanical

properties of the hydrogel samples were then compared by oscillatory rheometry (Figure 4g, h). Typically, two-component hydrogels where one component does not otherwise self-assemble tend to yield an alternate molecular packing, resulting in a stiffer hydrogel<sup>31</sup>. Here though, the characteristic frequency sweeps of this class of system were retained, and each forms a hydrogel of comparable stiffness, indicating that the inclusion of fucoidan (at this concentration) does not interfere with the processes that determine the final stiffness of the resultant hydrogels<sup>24a, 32</sup>.

#### *Interaction of fucoidan and the SAP fibrils*

To determine at the availability of the peptide sequence on the surface of the fibrils, we used <sup>1</sup>H NMR spectroscopic analysis. After addition of NaOH to solubilise the peptide (pH = 10), <sup>1</sup>H NMR provided a clean spectrum with narrow line widths. However, upon gelation, the resonances associated with the Fmoc- group and the fifth phenylalanine residue (F<sub>5</sub>) significantly broadened and was not visible. However, the dynamic motion of the RGDF–OH portion of the peptide is conserved in the fibrils, and resulted in narrow line widths for this portion of the peptide (Figure 3k). SANS measurements of fully hydrated samples of Fmoc-FRGDF and the co-assembled systems to investigate the nanostructures *in-situ* and to determine what effect the addition of fucoidan had on fibril radius. As SANS cannot distinguish features larger than approximately 17 nm under these conditions, the measurement was found to be insensitive to average fibril length. As SANS is sensitive to all structural features with sufficient contrast, we performed control measurements of 2 mg/mL fucoidan alone, which in 21.5% D<sub>2</sub>O, was found to provide conditions for negligible scattering from fucoidan. In the samples presented here we used these conditions to observe only the scattering from the fibrils as the contributions from fucoidan could complicate the analysis. This approach enabled the differences in the scattering between Fmoc-FRGDF and the co-

assembled system to be observed (Figure 3l). Analysis of the scattering data was performed using both a model-independent approach and a flexible cylinder model in the SASview package (supplementary information). The model-independent approach found that fibril radius for the 0RGD sample was  $48.8 \pm 0.9 \text{ \AA}$  with this value reducing to  $35.6 \pm 1.1 \text{ \AA}$  for 2RGD. Similar values were found using model fitting with the initial fibril radius of  $43.3 \pm 0.1 \text{ \AA}$ , reducing to  $33.7 \pm 0.1 \text{ \AA}$  when the peptide was co-assembled with fucoidan. These values are consistent with the diameter of the previously reported subunit of these assemblies<sup>29</sup>. The model fitting approach also indicated that there was a densification of the fibril after co-assembly with the scattering length density of the fibrils increasing by 9.6%.

We adapted a previously described method of gold nanoparticle (GNP) synthesis<sup>33</sup>, creating GNP labelled fucoidan which can be readily visualised with TEM (Figure 4d). Figures 4a-c show TEM micrographs of the nanofibrils in close association with the GNP labelled fucoidan. Two control hydrogels were prepared to control against possible associations between independent gold nanoparticles and either fucoidan or the peptide fibrils. One control hydrogel contained a mixture of unlabelled fucoidan and the independent GNP (Figure 4e), the other containing only the independent GNP (Figure 4f). All hydrogels were thoroughly washed with deionised water to remove any unbound nanoparticles from the hydrogel

Parallel plate rheometry was used to compare the rate of hydrogel formation<sup>34</sup>. When the materials were analysed after 48 hours, the final modulus were comparable across a range of frequencies, showed the final mechanical properties of the scaffolds were similar (Figure 4g). A fixed frequency time analysis showed that the co-assembled sample formed the hydrogel more rapidly with an order of magnitude increase in stiffness at a specific time (Figure 4h). Normalised isothermal titration calorimetry (ITC) thermograms (Figure 4i) was used to monitor the time taken for the Fmoc-FRGDF network formation (*i.e.* where the heat rate returns to zero), and the co-assembled sample showed a rate enhancement of *ca.* 40% in the

latter. Differential scanning calorimetry (DSC) analyses showed co-assembly increased  $T_{gel}$  from 90.1 °C. to 94.6 °C, while the post-assembly addition did not show a similar increase in  $T_{gel}$  (Figure 4j).

*Biological mechanism of the Fucoidan/Peptide Material.*

Immunostaining was performed on the cells cultured at 48 hours to capture the process mid cycle. SCC25 cells cultured on 0RGD were further counterstained with Hoechst dye to reveal NF $\kappa$ B p65 co-localised with the nuclear stain. When the same experiment was performed upon the 2RGD hydrogel, however, no significant staining of NF $\kappa$ B was observed.

To confirm that the material was effective at a gene expression level, we interrogated the mRNA regulation of genes in the NF $\kappa$ B pro-inflammatory pathway using quantitative PCR (see supplementary info. for primer sequences). RNA was extracted from the cells under both conditions and quantified for the gene expression studies. We included the pro-inflammatory cytokines interleukin (IL) 1A, 1B, 6, 8, and tissue necrotic factor (TNF), all transcribed as a key part of the NF $\kappa$ B pro-inflammatory pathway and were therefore monitored as crucial regulators of tumourigenesis (Figure 5c). The time point for studying gene expression was 48h. At this time point, most of the SCC25 cells remained viable (~70%). In each case, there was significant downregulation in the expression of each pro-inflammatory gene on 2RGD when compared to the control. In order to confirm that the down regulation of the anti-inflammatory cytokines was not related to apoptosis, the housekeeping gene ACTB was monitored and showed the same level of expression in both situations. Then, to test the extent of this effect, we then challenged the cells with LPS; as this challenge has been shown to increase expression even if the cells were apoptotic. In each gene analysed, the expression in the 0RGD system showed a significant increase, whereas the 2RGD was observed to be similar to the unchallenged sample.

## Discussion

The formation of stable, functional biomaterials that can present biologically active sequences and molecules will play a significant role in a range of medical applications. Self-assembly has been shown to give rise to materials that are both biocompatible and functional, but have not yet fully realised their potential. The use of simple interactions between these structures and additional functional molecules offers several advantages. The spontaneous formation of multicomponent scaffolds with defined chemical properties allows materials to be formed in physiological conditions, conferring inherent biocompatibility.

To ensure the material was biocompatible and non-toxic toward normal cell phenotypes, primary human mammary fibroblast cells (hMFC) were also cultured on the SAP hydrogels (Figure 2a). We chose these cell lines as fibroblasts and endothelial cancer cells have a close association in the tumour microenvironment<sup>35</sup>, and drugs that are solely cytotoxic also kill fibroblasts along with the target cells, a process which actually induces local tumourigenesis through the release of pro-cancerous factors<sup>5, 36</sup>. In addition, the correct presentation of RGD is a requirement for the culture of both cell types, as the SCC25 oral cancer cells show over expression of  $\alpha 5\beta 1$  integrin receptor<sup>37</sup>. The hMFC cells showed maintained equally high viability on both 0RGD and 2RGD, indicating that the inclusion of fucoidan did not negatively impact the cytotoxicity of the SAP matrix. However, the SCC25 cells showed significant numbers of dead cells in comparison. To verify that this mechanism was controlled apoptosis rather than necrosis, Annexin V staining was performed. Whilst no cells in the 0RGD hydrogel were apoptotic, the results revealed that the majority of cells cultured on the 2RGD hydrogels were in a late apoptotic phase, with only a few cells found to be in the early apoptotic phase. Confident that the fucoidan within the material contributed towards the reduction of the number of cancer cells through the induction of controlled apoptosis, we set

out to discover the mechanism by which it was distributed within the hydrogel. Ideally the material would retain the functional nanostructures formed by the Fmoc-SAP alone; however, the supramolecular ordering of self-assembled structures has been shown to be significantly altered in the presence of biological macromolecules such as proteins found in serum<sup>24b</sup> and the cytosol<sup>38</sup>, or when two or more complementary molecules are co-assembled<sup>31</sup>.

Using TEM and AFM analyses, we observed that the Fmoc-FRGDF formed a series of well-ordered bundles of striated nanofibrils underpinning a fibrous matrix (Figure 3a,e), which were very similar to those in the co-assembled sample, though a more pronounced bundling of fibrils was observed (Figure 3b,f). When the solution of fucoidan was examined, the analysis revealed the formation of a number of spherical structures with a diameter of ~20 nm (Figure 3c,g). Finally, for the post-assembled hydrogel, a mixture of structures was observed, where spherical structures similar to those observed in the fucoidan solution (sample 4) were distributed at high density over the fibrillar network at both the nano- and microscales (Figure 3 d,h).

To determine if the molecular packing of the Fmoc-SAP within the fibrils was affected by the fucoidan, a series of spectroscopic analyses were performed, as co-assemblies in general have been demonstrated to promote inconsistent alternative organisational structures<sup>24b, 38</sup>. The use of FTIR confirmed that the addition of fucoidan during the assembly process did not affect the molecular packing of the peptides into the desired anti-parallel  $\beta$ -sheets that drive these assemblies. Furthermore, the transitions observed via CD, shown to represent bundling between the fibrils driven by supramolecular interactions, are analogous to large macromolecules<sup>21, 30</sup>. Importantly, when the co-assembled material was compared to Fmoc-FRGDF, the wavelength of the transitions within the spectra was unchanged, but the magnitude was increased, suggesting the addition of fucoidan induced increased longitudinal

ordering (Figure 3j)<sup>30</sup>. Conversely, the magnitude of the transitions was diminished in the post-assembled sample, possibly as a result of disruptions arising from the mixing process, and potentially the unbound fucoidan forming aggregates increasing scattering in the far UV. The coassembly did not effect the mechanical properties of the resultant hydrogels; when the mechanical properties of the hydrogels were studied, the characteristic frequency sweeps of this class of system were retained, and each forms a hydrogel of comparable stiffness. Typically, two-component hydrogels where one component does not otherwise self-assemble tend to yield an alternate molecular packing, resulting in a stiffer hydrogel<sup>31</sup>, indicating that the inclusion of fucoidan (at this concentration) does not interfere with the processes that determine the final stiffness of the resultant hydrogels<sup>24a, 32</sup>.

We hypothesised that the mechanism by which the fucoidan in the co-assembled sample was incorporated into the fibrillar network was through non-covalent interactions with amino acid(s) present on the surface of the fibrils. NMR data suggests restricted movement of the Fmoc and first phenylalanine due to assembly into nanotubes<sup>29</sup>. However, the dynamic motion of the RGDF–OH portion of the peptide is conserved in the fibrils and resulted in narrow line widths for this portion of the peptide. By integrating <sup>1</sup>H NMR resonances, it was concluded that <5 % of the RGD portion of the peptide was available in solution, and therefore available for interaction. . It has been shown that a minimum spacing of ~440nm between RGD epitopes is sufficient for effective cell attachment<sup>39</sup>, and the most effective cell interaction is achieved with well spaced clustered of epitopes<sup>40</sup>. As the entire fibril consists of closely packed fmoc-FRGDF peptides, the limited availability of the RGD portion on the surface of the fibrils may in fact contribute to the observed cell attachment properties<sup>18a</sup>. We then employed small angle neutron scattering (SANS) analysis to look at the effect of the interaction with fucoidan on the fibril morphology. Although a slight reduction in radius is observed, the scattering fit suggests that the morphology of the fibril is broadly retained, as

opposed to the formation of a secondary, self-sorted structure<sup>41</sup>. This retention of morphology coupled with an increase in density suggests that the fucoidan interaction is allowing the SAP fibril structure and morphology to be broadly retained, but is having an effect on the fibrils. This co-localisation was confirmed by physically observing the location of fucoidan by labelling it with a gold nanoparticle that could be observed via TEM. After washing, GNP remained present only with the GNP labelled fucoidan, where they were observed in close association with the peptide fibrils. This indicated a strong and persistent co-localisation of the fucoidan to the fibrils.

We observed that the co-assembled sample formed more quickly, possibly due to the bundling and co-location providing an increased driving force for assembly. In order to analyse the effects of this driving force on the time it takes the gel network to form, we used parallel plate rheometry to compare the rate of hydrogel formation<sup>34</sup>. When the materials were analysed after 48 hours, the final modulus were comparable across a range of frequencies, suggesting the final mechanical properties of the scaffolds were similar (Figure 4g). However, a fixed frequency time analysis showed that the co-assembled sample formed the hydrogel more rapidly (Figure 4h). We then analysed the sol-gel transition temperature ( $T_{gel}$ ) to determine possible effects of this stabilisation on the melting temperature of the hydrogels using a series of DSC analysis. These observations suggest further that the co-assembly process leads to a stabilisation of the interfibrillar network. These results suggests that the fucoidan is enhancing the stability of the fibrils in the co-assembled system by increasing supramolecular order<sup>30</sup>, albeit without significantly increasing its stiffness (Figure 4g).

Confident in the structure of our material, we decided to further probe its effect on the oral cancer cell line in further detail. Previous studies of the SCC25 cell line in comparison with normal human oral keratinocytes revealed significant over expression of the pro-inflammatory

cytokine response, upregulation of the cytokinesis promoting genes<sup>42</sup> and, in particular, increased expression of NF $\kappa$ B useful here as an easily characterised component of a larger inflammatory pathway<sup>43</sup>. The uncontrolled G2 to M cell cycle progression is essential for oral cancer progression, and is characterised by an increase in the tumour size<sup>43</sup>. The transcription factors associated with this pathway, PLK1 and FOXM1, activate CEP55, a cytokinesis promoter identified as a key marker of tumor formation and progression<sup>44</sup>. Earlier CEP55 knockdown studies have revealed a reduction in cell proliferation and tumorigenicity of the cancer cells<sup>45</sup>. In addition, to further test the material and model the highly pro-inflammatory environment of the tumour, the cells were challenged with lipopolysaccharide (LPS), a powerful inflammatory agent, providing a valid assay for the progression of these cancer cell lines<sup>46</sup>. To investigate the mechanism inducing selective apoptotic effects in the cancer cells observed earlier (Figure 2) we performed a series of experiments to monitor the observed effects of the material on the protein expression of NF $\kappa$ B and CEP55 (Figure 5a,b). When the same experiment was performed upon the 2RGD hydrogel, however, no significant staining of NF $\kappa$ B was observed suggests that the material results in a significant reduction in the protein expression of NF $\kappa$ B when compared to those stimulated by LPS. As expected, significant CEP55 protein expression was observed in SCC25 cells on the 0RGD hydrogel whereas the cells cultured on 2RGD hydrogels demonstrated little or no CEP55 protein expression, significantly this process was irrespective of stimulation with LPS, indicating that cytokinesis was effectively inhibited by the immobilised fucoidan (Figure 5a,b). We then confirmed these observations with gene expression studies. As expected, when SCC25 cells were cultured on 0RGD with LPS, the response of each of the pro-inflammatory cytokines was significantly up regulated. However, when the same conditions were applied to the 2RGD hydrogel, there was a significant inhibition in the transcription of each of the cytokine promoting genes. Importantly, the expression in each of the cytokines analysed was significantly less than that observed in the control, and comparable to the unchallenged 2RGD

sample.  $\text{NF}\kappa\text{B}$  suppresses apoptosis by inducing the expression of a number of anti-apoptotic genes whose products include inhibitors of apoptosis (IAPs), and TNF receptor associated factor 1 (TRAF1) and TRAF2<sup>47</sup>. The mechanism behind the effect of this material could be due to the reduced activation and expression of anti-apoptotic products which protect the cells from apoptosis by blocking the apoptotic cascade and/or regulate other anti-apoptotic pathways<sup>48</sup>. We studied the materials potential as an effective anti-mitogenic agent<sup>12a</sup>. As shown in Figure 5c, when the SCC25 cells were cultured on 2RGD compared to 0RGD a significant downregulation of CEP55 mRNA expression was observed, again irrespective of LPS stimulation, as observed in the protein expression studies. However, when LPS was used to stimulate cells cultured on 0RGD hydrogel, a significant 50-fold inhibition of the CEP55 gene was observed with the 2RGD hydrogel. Therefore, the gene and protein data indicate that the inclusion of fucoidan allows the hydrogel to act as a powerful inhibitor of cytokinesis and the uncontrolled cell proliferation associated with this type of cancer, and potentially many others. We have shown for the first time that the self-assembly process is able to present a bioactive macromolecule, the anti-inflammatory polysaccharide fucoidan, so that the scaffold provides a non-toxic, biocompatible, yet potent environment to potentially treat a range of pro-inflammatory cancers. Future work in our laboratory will extend this study to other cell lines, and *in-vivo* studies. We suggest that this method to form materials can easily be adapted to treat a range of other disease states. We foresee that this simple yet powerful approach will develop further to allow researchers the convenient fabrication of inexpensive but complex materials which can be easily directed toward specific therapeutic outcomes.

**Acknowledgements:** This work was funded by an Australian Research Council (ARC) Discovery Project (DP130103131). NMR instrumentation was provided through ARC funding (LE110100141). DRN was supported by an NHMRC Career Development

Fellowship (APP1050684). RJW was supported *via* an Alfred Deakin Research Fellowship. Access to the facilities of the Centre for Advanced Microscopy (CAM) with funding through the Australian Microscopy and Microanalysis Research Facility (AMMRF) is gratefully acknowledged. AJCD was supported by the Swedish Research Council VR. Preliminary SANS measurements were performed at the Low Energy Neutron Source, Indiana. Access to the D33 instrument was provided by the Institut Laue-Langevin user access programme (8-03-826).

## References

1. Ferrari, M., Cancer nanotechnology: opportunities and challenges. *Nature Reviews Cancer* **2005**, *5* (3), 161-171.
2. Quail, D. F.; Joyce, J. A., Microenvironmental regulation of tumor progression and metastasis. *Nat Med* **2013**, *19* (11), 1423-1437.
3. (a) Grivennikov, S. I.; Greten, F. R.; Karin, M., Immunity, inflammation, and cancer. *Cell* **2010**, *140* (6), 883-899; (b) Conde, J.; Bao, C.; Tan, Y.; Cui, D.; Edelman, E. R.; Azevedo, H. S.; Byrne, H. J.; Artzi, N.; Tian, F., Dual Targeted Immunotherapy via In Vivo Delivery of Biohybrid RNAi-Peptide Nanoparticles to Tumor-Associated Macrophages and Cancer Cells. *Advanced Functional Materials* **2015**, n/a-n/a.
4. Cox, T. R.; Erler, J. T., Remodeling and homeostasis of the extracellular matrix: implications for fibrotic diseases and cancer. *Disease Models & Mechanisms* **2011**, *4* (2), 165-178.
5. Coussens, L. M.; Werb, Z., Inflammation and cancer. *Nature* **2002**, *420* (6917), 860-867.
6. (a) Jones, M. K.; Wang, H.; Peskar, B. M.; Levin, E.; Itani, R. M.; Sarfeh, I. J.; Tarnawski, A. S., Inhibition of angiogenesis by nonsteroidal anti-inflammatory drugs: insight into mechanisms and implications for cancer growth and ulcer healing. *Nature medicine* **1999**, *5* (12), 1418-1423; (b) Cuzick, J.; Otto, F.; Baron, J. A.; Brown, P. H.; Burn, J.; Greenwald, P.; Jankowski, J.; La Vecchia, C.; Meyskens, F.; Senn, H. J., Aspirin and non-steroidal anti-inflammatory drugs for cancer prevention: an international consensus statement. *The lancet oncology* **2009**, *10* (5), 501-507.
7. (a) Yallapu, M. M.; Jaggi, M.; Chauhan, S. C., Design and engineering of nanogels for cancer treatment. *Drug discovery today* **2011**, *16* (9), 457-463; (b) Drury, J. L.; Mooney, D. J., Hydrogels for tissue engineering: scaffold design variables and applications. *Biomaterials* **2003**, *24* (24), 4337-4351.
8. Wolinsky, J. B.; Colson, Y. L.; Grinstaff, M. W., Local drug delivery strategies for cancer treatment: gels, nanoparticles, polymeric films, rods, and wafers. *Journal of Controlled Release* **2012**, *159* (1), 14-26.
9. Geiger, B.; Bershadsky, A.; Pankov, R.; Yamada, K. M., Transmembrane crosstalk between the extracellular matrix and the cytoskeleton. *Nature Reviews Molecular Cell Biology* **2001**, *2* (11), 793-805.
10. Whitesides, G. M.; Boncheva, M., Beyond molecules: Self-assembly of mesoscopic and macroscopic components. *Proc. Natl. Acad. Sci. U. S. A.* **2002**, *99* (8), 4769-4774.
11. (a) Dias, P. F.; Siqueira Jr, J. M.; Vendruscolo, L. F.; de Jesus Neiva, T.; Gagliardi, A. R.; Maraschin, M.; Ribeiro-do-Valle, R. M., Antiangiogenic and antitumoral properties of a

polysaccharide isolated from the seaweed *Sargassum stenophyllum*. *Cancer chemotherapy and pharmacology* **2005**, *56* (4), 436-446; (b) Kim, E. J.; Park, S. Y.; Lee, J.-Y.; Park, J. H., Fucoidan present in brown algae induces apoptosis of human colon cancer cells. *BMC gastroenterology* **2010**, *10* (1), 96.

12. (a) Patel, M. K.; Mulloy, B.; Gallagher, K. L.; O'Brien, L.; Hughes, A. D., The antimitogenic action of the sulphated polysaccharide fucoidan differs from heparin in human vascular smooth muscle cells. *Thrombosis and haemostasis* **2002**, *87* (1), 149-54; (b) Park, H. Y.; Kim, G. Y.; Moon, S. K.; Kim, W. J.; Yoo, Y. H.; Choi, Y. H., Fucoidan inhibits the proliferation of human urinary bladder cancer t24 cells by blocking cell cycle progression and inducing apoptosis. *Molecules (Basel, Switzerland)* **2014**, *19* (5), 5981-98.

13. Zhu, C.; Cao, R.; Zhang, S. X.; Man, Y. N.; Wu, X. Z., Fucoidan inhibits the growth of hepatocellular carcinoma independent of angiogenesis. *Evidence-based complementary and alternative medicine : eCAM* **2013**, *2013*, 692549.

14. Murakami, K.; Aoki, H.; Nakamura, S.; Nakamura, S.-i.; Takikawa, M.; Hanzawa, M.; Kishimoto, S.; Hattori, H.; Tanaka, Y.; Kiyosawa, T.; Sato, Y.; Ishihara, M., Hydrogel blends of chitin/chitosan, fucoidan and alginate as healing-impaired wound dressings. *Biomaterials* **2010**, *31* (1), 83-90.

15. Sezer, A. D.; Hatipoglu, F.; Cevher, E.; Oğurtan, Z.; Bas, A. L.; Akbuğa, J., Chitosan film containing fucoidan as a wound dressing for dermal burn healing: preparation and in vitro/in vivo evaluation. *AAPS PharmSciTech* **2007**, *8* (2), 1530-9932.

16. Worthington, P.; Pochan, D. J.; Langhans, S. A., Peptide hydrogels – versatile matrices for 3D cell culture in cancer medicine. *Frontiers in Oncology* **2015**, *5*.

17. Rodriguez, A. L.; Wang, T. Y.; Bruggeman, K. F.; Horgan, C. C.; Li, R.; Williams, R. J.; Parish, C. L.; Nisbet, D. R., In vivo assessment of grafted cortical neural progenitor cells and host response to functionalized self-assembling peptide hydrogels and the implications for tissue repair. *Journal of Materials Chemistry B* **2014**, *2* (44), 7771-7778.

18. (a) Modepalli, V. N.; Rodriguez, A. L.; Li, R.; Pavuluri, S.; Nicholas, K. R.; Barrow, C. J.; Nisbet, D. R.; Williams, R. J., In vitro response to functionalized self - assembled peptide scaffolds for three - dimensional cell culture. *Peptide Science* **2014**, *102* (2), 197-205; (b) Zhou, M.; Smith, A. M.; Das, A. K.; Hodson, N. W.; Collins, R. F.; Ulijn, R. V.; Gough, J. E., Self-assembled peptide-based hydrogels as scaffolds for anchorage-dependent cells. *Biomaterials* **2009**, *30* (13), 2523-2530.

19. (a) Nisbet, D.; Williams, R., Self-Assembled Peptides: Characterisation and In Vivo Response. *Biointerphases* **2012**, *7* (1), 1-14; (b) Boekhoven, J.; Stupp, S. I., 25th Anniversary Article: Supramolecular Materials for Regenerative Medicine. *Advanced Materials* **2014**.

20. Rodriguez, A.; Wang, T.-Y.; Bruggeman, K.; Li, R.; Williams, R.; Parish, C.; Nisbet, D., Tailoring minimalist self-assembling peptides for localized viral vector gene delivery. *Nano Res.* **2015**, 1-11.

21. Williams, R. J.; Smith, A. M.; Collins, R.; Hodson, N.; Das, A. K.; Ulijn, R. V., Enzyme-assisted self-assembly under thermodynamic control. *Nature Nanotechnology* **2009**, *4* (1), 19-24.

22. Rodriguez, A. L.; Parish, C. L.; Nisbet, D. R.; Williams, R. J., Tuning the amino acid sequence of minimalist peptides to present biological signals via charge neutralised self assembly. *Soft Matter* **2013**, *9*, 3915-3919.

23. Li, R.; Horgan, C. C.; Long, B.; Rodriguez, A. L.; Mather, L.; Barrow, C. J.; Nisbet, D. R.; Williams, R. J., Tuning the mechanical and morphological properties of self-assembled peptide hydrogels via control over the gelation mechanism through regulation of ionic strength and the rate of pH change. *RSC Advances* **2015**, *5* (1), 301-307.

24. (a) Williams, R. J.; Hall, T. E.; Glattauer, V.; White, J.; Pasic, P. J.; Sorensen, A. B.; Waddington, L.; McLean, K. M.; Currie, P. D.; Hartley, P. G., The in vivo performance of an enzyme-assisted self-assembled peptide/protein hydrogel. *Biomaterials* **2011**, *32* (22), 5304-

- 5310; (b) Javid, N.; Roy, S.; Zelzer, M.; Yang, Z.; Sefcik, J.; Ulijn, R. V., Cooperative Self-Assembly of Peptide Gelators and Proteins. *Biomacromolecules* **2013**, *14* (12), 4368-4376.
25. (a) Zhao, F.; Ma, M. L.; Xu, B., Molecular hydrogels of therapeutic agents. *Chem. Soc. Rev.* **2009**, *38* (4), 883-891; (b) Yang, Z. M.; Xu, K. M.; Wang, L.; Gu, H. W.; Wei, H.; Zhang, M. J.; Xu, B., Self-assembly of small molecules affords multifunctional supramolecular hydrogels for topically treating simulated uranium wounds. *Chem. Commun.* **2005**, (35), 4414-4416; (c) Bhuniya, S.; Seo, Y. J.; Kim, B. H., Ibuprofen-based hydrogelators: an approach toward anti-inflammatory drug delivery. *Tetrahedron letters* **2006**, *47* (40), 7153-7156.
26. Dewhurst, C. D., D33 - a third small-angle neutron scattering instrument at the Institut Laue Langevin. *Measurement Science & Technology* **2008**, *19* (3), 8.
27. Kline, S. R., Reduction and analysis of SANS and USANS data using IGOR Pro. *Journal of Applied Crystallography* **2006**, *39*, 895-900.
28. Rheinwald, J. G.; Beckett, M. A., Tumorigenic keratinocyte lines requiring anchorage and fibroblast support cultured from human squamous cell carcinomas. *Cancer Res* **1981**, *41* (5), 1657-63.
29. Smith, A. M.; Williams, R. J.; Tang, C.; Coppo, P.; Collins, R. F.; Turner, M. L.; Saiani, A.; Ulijn, R. V., Fmoc-Diphenylalanine self assembles to a hydrogel via a novel architecture based on pi-pi interlocked beta-sheets. *Advanced Materials* **2008**, *20* (1), 37-41.
30. Hirst, A. R.; Roy, S.; Arora, M.; Das, A. K.; Hodson, N.; Murray, P.; Marshall, S.; Javid, N.; Sefcik, J.; Boekhoven, J.; van Esch, J. H.; Santabarbara, S.; Hunt, N. T.; Ulijn, R. V., Biocatalytic induction of supramolecular order. *Nat Chem* **2010**, *2* (12), 1089-1094.
31. Raeburn, J.; Adams, D. J., Multicomponent low molecular weight gelators. *Chem. Commun.* **2014**.
32. (a) Adams, D. J. F., W.F. Kirkland, M. Mullen, L. Sanderson, P., Tailoring Gel Strength by Amino Acid Sequence in Fmoc Dipeptide Hydrogels. *Soft Matter* **2009**, *5*, 1856 - 1862; (b) Cheng, G.; Castelletto, V.; Moulton, C. M.; Newby, G. E.; Hamley, I. W., Hydrogelation and Self-Assembly of Fmoc-Tripeptides: Unexpected Influence of Sequence on Self-Assembled Fibril Structure, and Hydrogel Modulus and Anisotropy. *Langmuir* **2010**, *26* (7), 4990-4998.
33. Lirdprapamongkol, K.; Warisnoicharoen, W.; Soisuwan, S.; Svasti, J., Eco-friendly synthesis of fucoidan-stabilized gold nanoparticles. *American Journal of Applied Sciences* **2010**, *7* (8), 1038.
34. Williams, R. J.; Gardiner, J.; Sorensen, A. B.; Marchesan, S.; Mulder, R. J.; McLean, K. M.; Hartley, P. G., Monitoring the Early Stage Self-Assembly of Enzyme-Assisted Peptide Hydrogels. *Australian Journal of Chemistry* **2013**, *66* (5), 572-578.
35. Sayes, C. M.; Wahi, R.; Kurian, P. A.; Liu, Y.; West, J. L.; Ausman, K. D.; Warheit, D. B.; Colvin, V. L., Correlating nanoscale titania structure with toxicity: a cytotoxicity and inflammatory response study with human dermal fibroblasts and human lung epithelial cells. *Toxicological Sciences* **2006**, *92* (1), 174-185.
36. (a) Kalluri, R.; Zeisberg, M., Fibroblasts in cancer. *Nature Reviews Cancer* **2006**, *6* (5), 392-401; (b) Olumi, A. F.; Grossfeld, G. D.; Hayward, S. W.; Carroll, P. R.; Tlsty, T. D.; Cunha, G. R., Carcinoma-associated fibroblasts direct tumor progression of initiated human prostatic epithelium. *Cancer research* **1999**, *59* (19), 5002-5011.
37. Hamill, K. J.; Hopkinson, S. B.; Hoover, P.; Todorović, V.; Green, K. J.; Jones, J. C., Fibronectin expression determines skin cell motile behavior. *Journal of Investigative Dermatology* **2012**, *132* (2), 448-457.
38. Kuang, Y.; Yuan, D.; Zhang, Y.; Kao, A.; Du, X.; Xu, B., Interactions between cellular proteins and morphologically different nanoscale aggregates of small molecules. *RSC Advances* **2013**, *3* (21), 7704-7707.

39. Massia, S. P.; Hubbell, J. A., An RGD spacing of 440 nm is sufficient for integrin alpha V beta 3-mediated fibroblast spreading and 140 nm for focal contact and stress fiber formation. *The Journal of cell biology* **1991**, *114* (5), 1089-1100.
40. Maheshwari, G.; Brown, G.; Lauffenburger, D. A.; Wells, A.; Griffith, L. G., Cell adhesion and motility depend on nanoscale RGD clustering. *Journal of Cell Science* **2000**, *113* (10), 1677-1686.
41. Morris, K. L.; Chen, L.; Raeburn, J.; Sellick, O. R.; Cotanda, P.; Paul, A.; Griffiths, P. C.; King, S. M.; O'Reilly, R. K.; Serpell, L. C.; Adams, D., Chemically programmed self-sorting of gelator networks. *Nature communications* **2013**, *4*, 1480.
42. (a) Nakano, Y.; Kobayashi, W.; Sugai, S.; Kimura, H.; Yagihashi, S., Expression of tumor necrosis factor-alpha and interleukin-6 in oral squamous cell carcinoma. *Japanese journal of cancer research : Gann* **1999**, *90* (8), 858-66; (b) Reuter, S.; Charlet, J.; Juncker, T.; Teiten, M. H.; Dicato, M.; Diederich, M., Effect of curcumin on nuclear factor kappaB signaling pathways in human chronic myelogenous K562 leukemia cells. *Annals of the New York Academy of Sciences* **2009**, *1171*, 436-47.
43. Rao, S. K.; Pavicevic, Z.; Du, Z.; Kim, J. G.; Fan, M.; Jiao, Y.; Rosebush, M.; Samant, S.; Gu, W.; Pfeffer, L. M.; Nosrat, C. A., Pro-inflammatory genes as biomarkers and therapeutic targets in oral squamous cell carcinoma. *The Journal of biological chemistry* **2010**, *285* (42), 32512-21.
44. Waseem, A.; Ali, M.; Odell, E. W.; Fortune, F.; Teh, M. T., Downstream targets of FOXM1: CEP55 and HELLS are cancer progression markers of head and neck squamous cell carcinoma. *Oral oncology* **2010**, *46* (7), 536-42.
45. Tao, J.; Zhi, X.; Tian, Y.; Li, Z.; Zhu, Y.; Wang, W.; Xie, K.; Tang, J.; Zhang, X.; Wang, L.; Xu, Z., CEP55 contributes to human gastric carcinoma by regulating cell proliferation. *Tumour biology : the journal of the International Society for Oncodevelopmental Biology and Medicine* **2014**, *35* (5), 4389-99.
46. Ko, S. C.; Huang, C. R.; Shieh, J. M.; Yang, J. H.; Chang, W. C.; Chen, B. K., Epidermal growth factor protects squamous cell carcinoma against cisplatin-induced cytotoxicity through increased interleukin-1beta expression. *PloS one* **2013**, *8* (2), e55795.
47. Lin, A.; Karin, M. In *NF- $\kappa$ B in cancer: a marked target*, Seminars in cancer biology, Elsevier: 2003; pp 107-114.
48. Yamamoto, Y.; Gaynor, R. B., Therapeutic potential of inhibition of the NF- $\kappa$ B pathway in the treatment of inflammation and cancer. *Journal of Clinical investigation* **2001**, *107* (2), 135.
49. Yu, C.; Young, S.; Russo, V.; Amsden, B. G.; Flynn, L. E., Techniques for the isolation of high-quality RNA from cells encapsulated in chitosan hydrogels. *Tissue engineering. Part C, Methods* **2013**, *19* (11), 829-38.

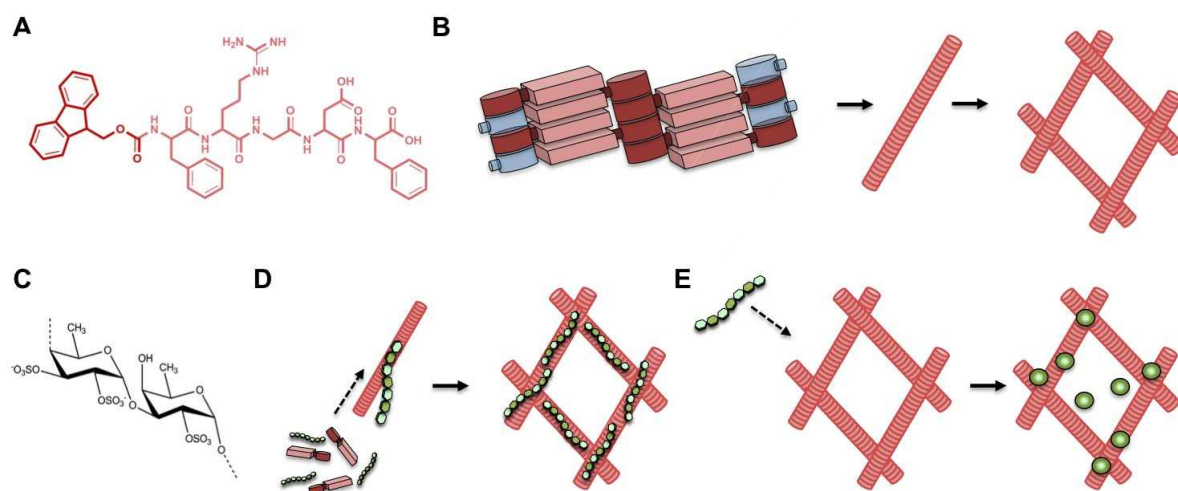


**Figure 1. Cartoon of the coassembly mechanism** A) structure of Fmoc-FRGDF, B) cartoon schematic showing the  $\pi$  stacking of Fmoc and the antiparallel interactions of the peptide which drive its assembly to fibrils that intertwine to form a scaffold, C) structure of a fucoidan subunit, D) co-assembly results in an interaction of fucoidan with fibrils, resulting in the presentation of the molecule over the surface of the scaffold. E) the addition of fucoidan post-assembly however does not produce a surface decorated structure, instead it results in the formation of separate disordered fucoidan aggregates.

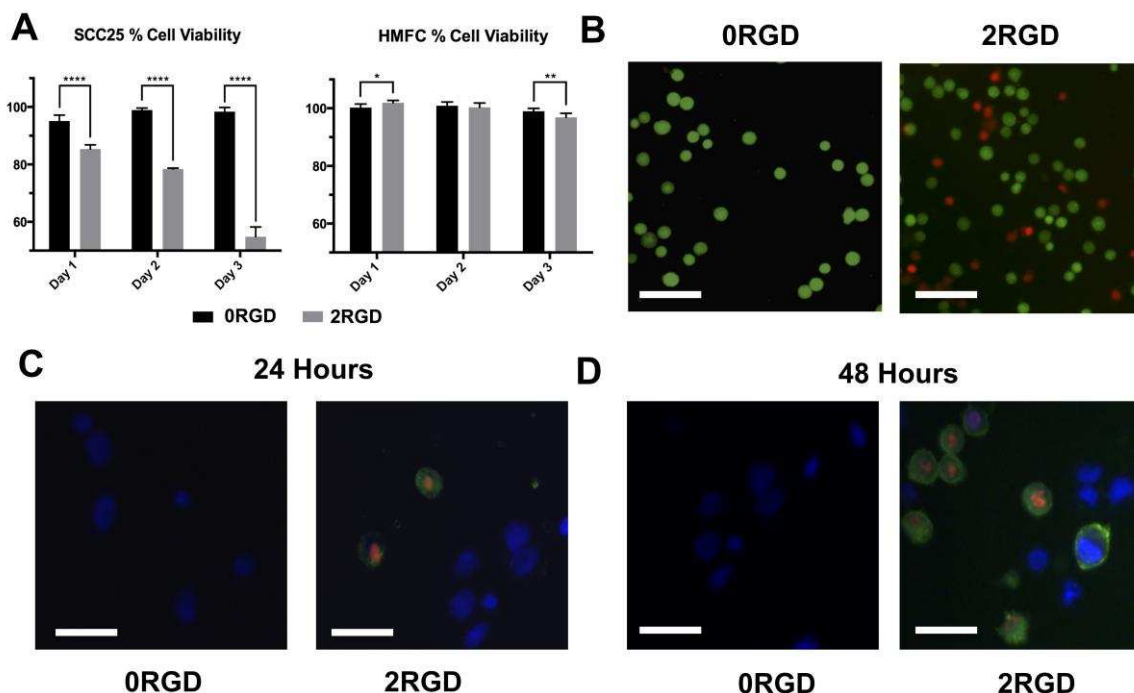


**Figure 2. Biocompatibility and the effect of the material on Cancer (SCC25) and healthy (hMFC) cell fate.** A) the shows the relative viabilities of the cells on each scaffold over three days. SCC25 cells were seeded on the Fmoc-FRGDF hydrogel (0RGD) and 2 mg/mL fucoidan (2RGD) and incubated for 3 days. Calcein AM staining was performed to identify live cells (green) and propidium iodide was used to identify dead cells (red). Scale bars 125 $\mu$ m. A minimum of 5 fields were captured for each treatment and number of live cells and dead cells were counted individually and percentage was calculated \*  $p = 0.05$ , \*\*  $p = 0.01$ , \*\*\*  $p = 0.001$  \*\*\*\*  $p = 0.0001$ . (n=3) B). shows the distribution of SCC25 cells on day 3 on each hydrogel C and D) Apoptosis at 24 and 48 hours. In order to determine the mode of cell death in the SCC25 cells, we stained the cells using Annexin V (green), Propidium iodide (red) and Hoechst dye (blue). Live cells are identified by a nucleus stained only with hoechst dye and appear only blue Early apoptotic cells were stained green with nucleus blue and the late apoptotic cells stained in green with a red nucleus. Scale bars 50 $\mu$ m.

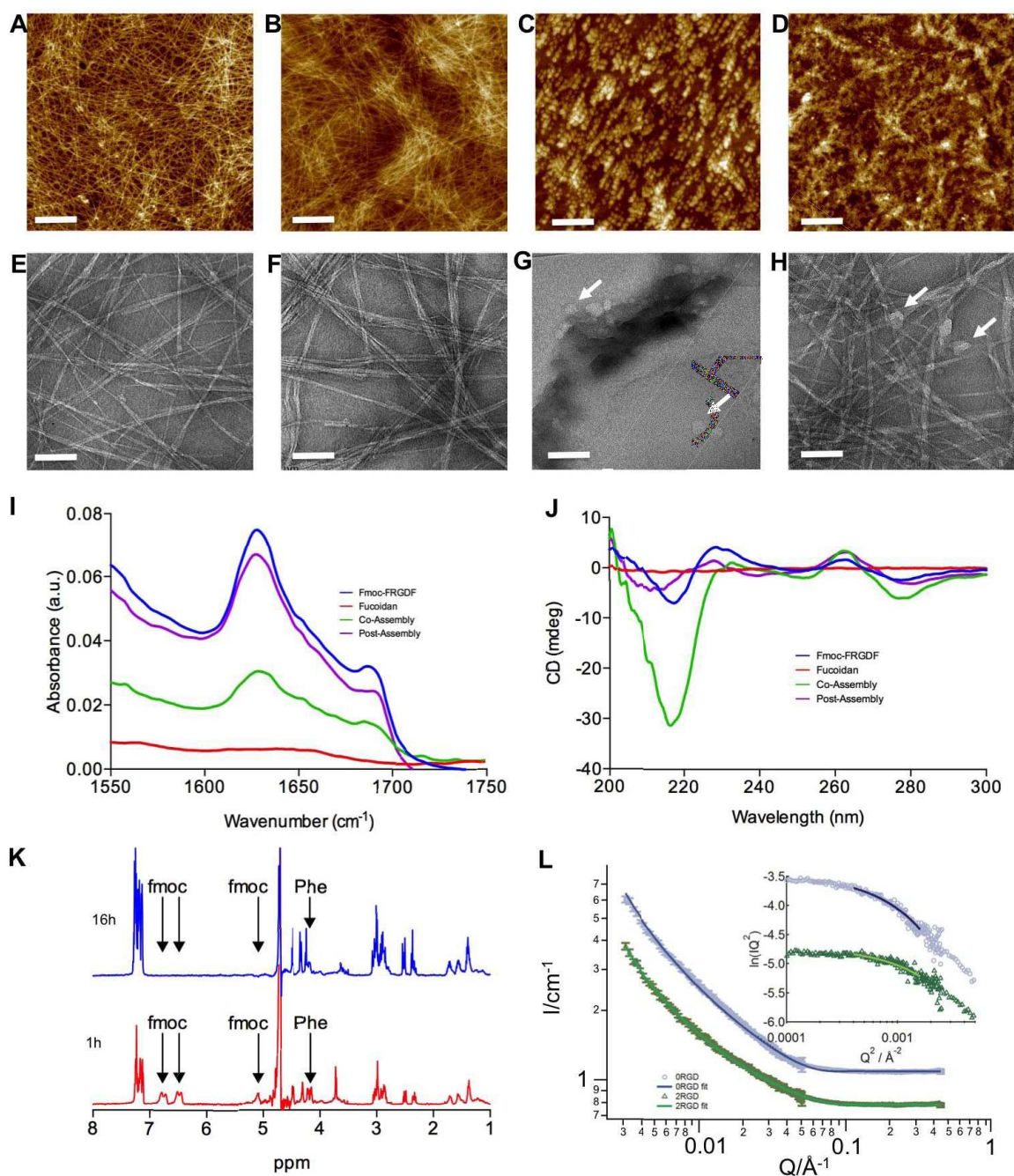


**Figure 3: The underpinning structure and organisation of the scaffold.** AFM microscopy shows the structures formed by A) Fmoc-FRGDF, B) co-assembled with 2 mg/mL fucoidan, C) a solution of fucoidan D) post addition fucoidan (scale bar represents 1  $\mu\text{m}$ ). E-F) equivalent via negatively stained TEM. G) shows aggregates of fucoidan, which are similar to structures visible in post addition H), but not co-assembly F) (scale bar represents 75 nm). I) FTIR shows conserved antiparallel  $\beta$ -sheet formation. Fucoidan solution shows no overall structure. J) CD shows increased supramolecular ordering of Fmoc-FRDGF when co-assembled. The transitions characteristic to this class of assembly are maintained across all the SAP containing samples, indicating the same chiral structure dominates. Co-assembly increases the magnitude of the transitions indicating an increase in supramolecular ordering whereas post-assembly disrupts structure. The solution of fucoidan has no overriding chiral signal. K) NMR analysis shows that upon assembly Fmoc is completely removed from solution and the N-terminal (i.e. closets to Fmoc) Phe is partially removed from solution as the assembly forms, indicating that the RGDf portion is still in solution, and presented on the surface of the assemblies. L) Analysis of SANS using both a flexible cylinder model and model-independent Kratky analysis (inset) of the data show a reduction in the fibril radius when co-assembled with fucoidan. Plots are offset for clarity.

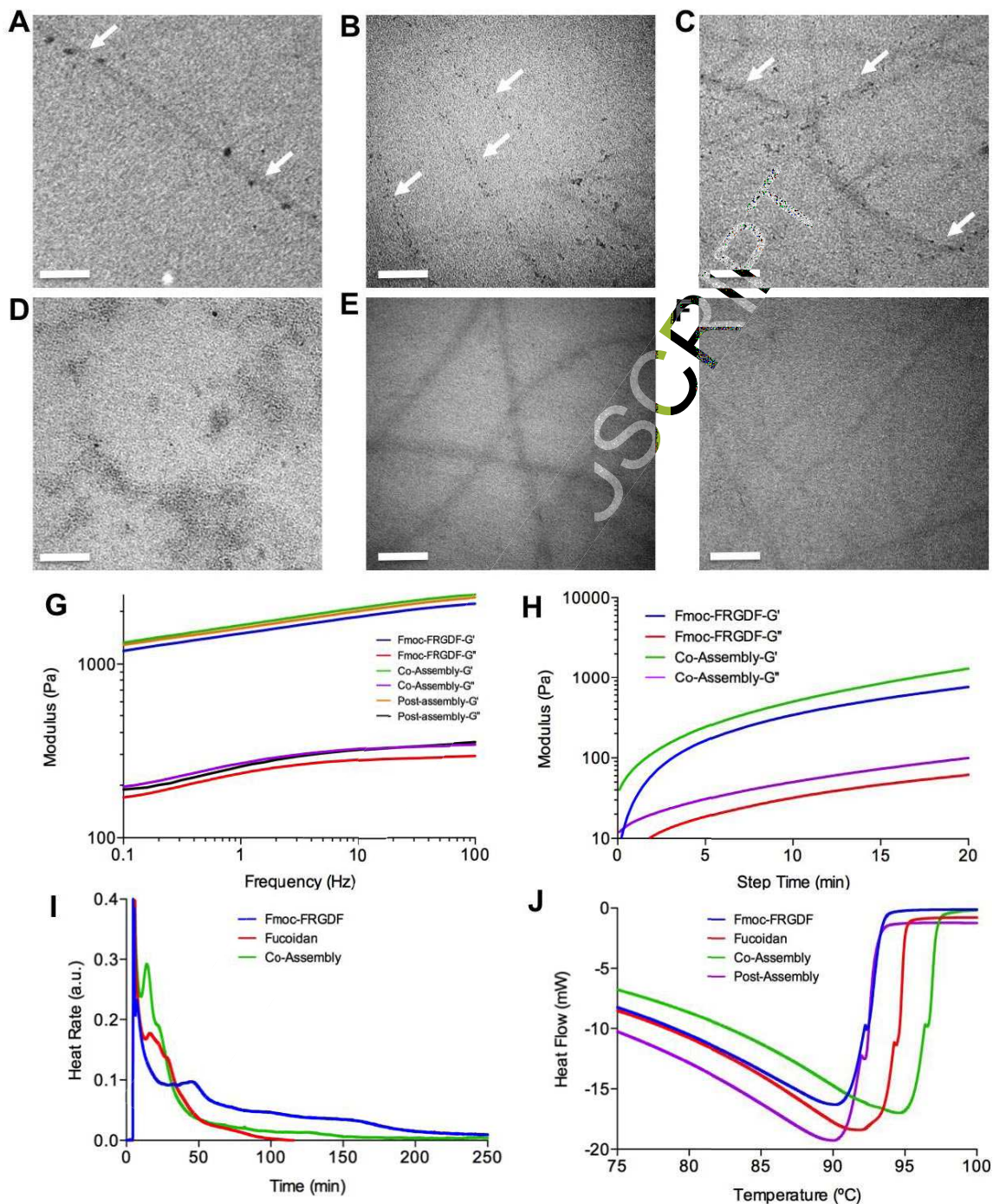


**Figure 4. Location of fucoidan in relation to the fibrils and the effects on the final hydrogel:** GNP labelled fucoidan shows co-localisation along peptide fibrils A) pre and B,C) post washing of the hydrogel indicating strong associations between fucoidan and peptide fibrils. D) GNP labelled fucoidan in solution. E) hydrogel co-assembled with unlabelled fucoidan and independent GNP show no residual GNP post washing. F) hydrogel co-assembled only with independent GNP show no residual GNP post washing (scale bar represents 100 nm). G) rheological characteristics of hydrogels. H) rate of formation of hydrogel is increased in co-assembly. I) ITC shows increased rate of assembly with co-assembled samples (return of heat rate to 0). J) DSC shows increased melting temperature of co-assembled system.

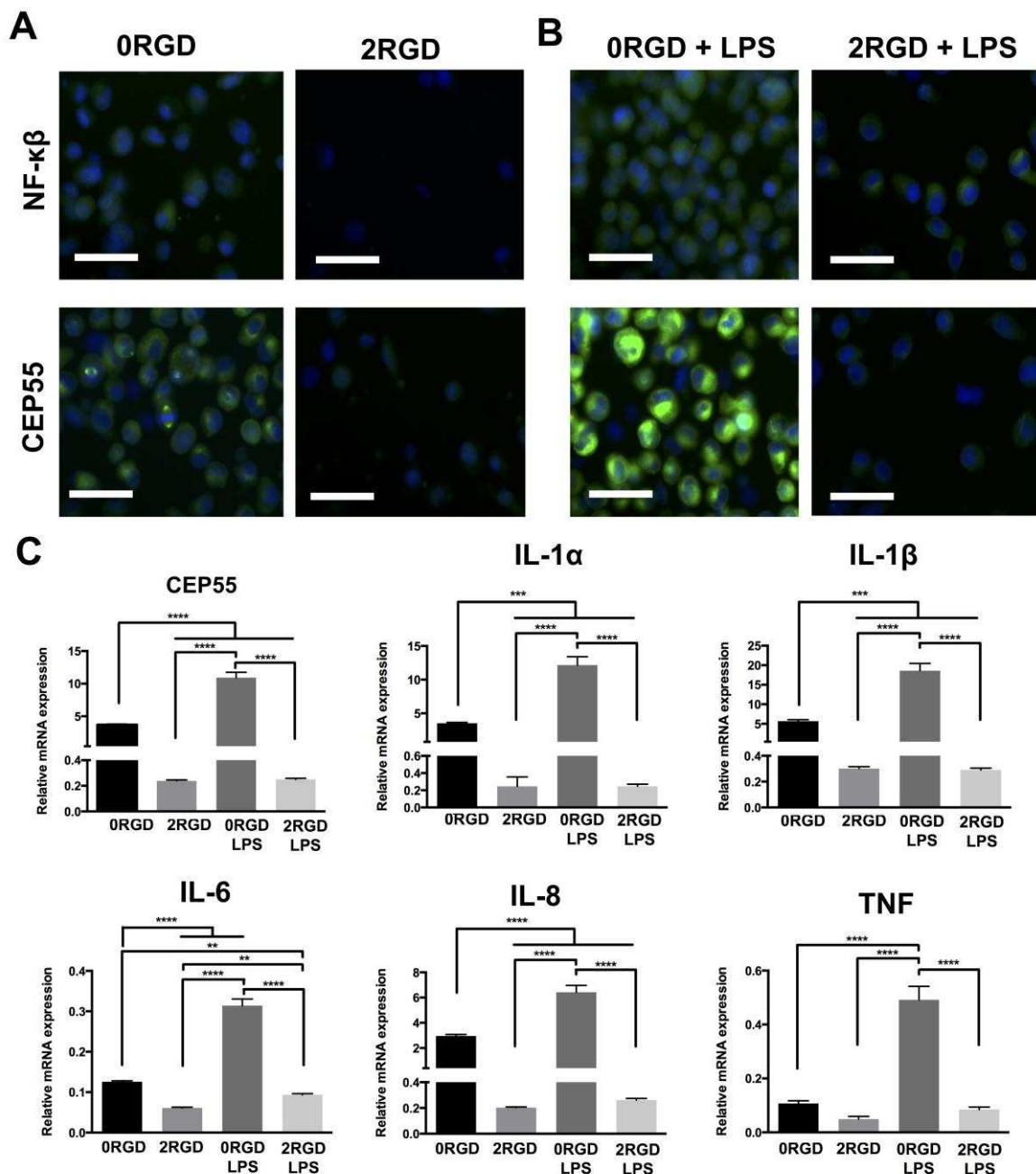
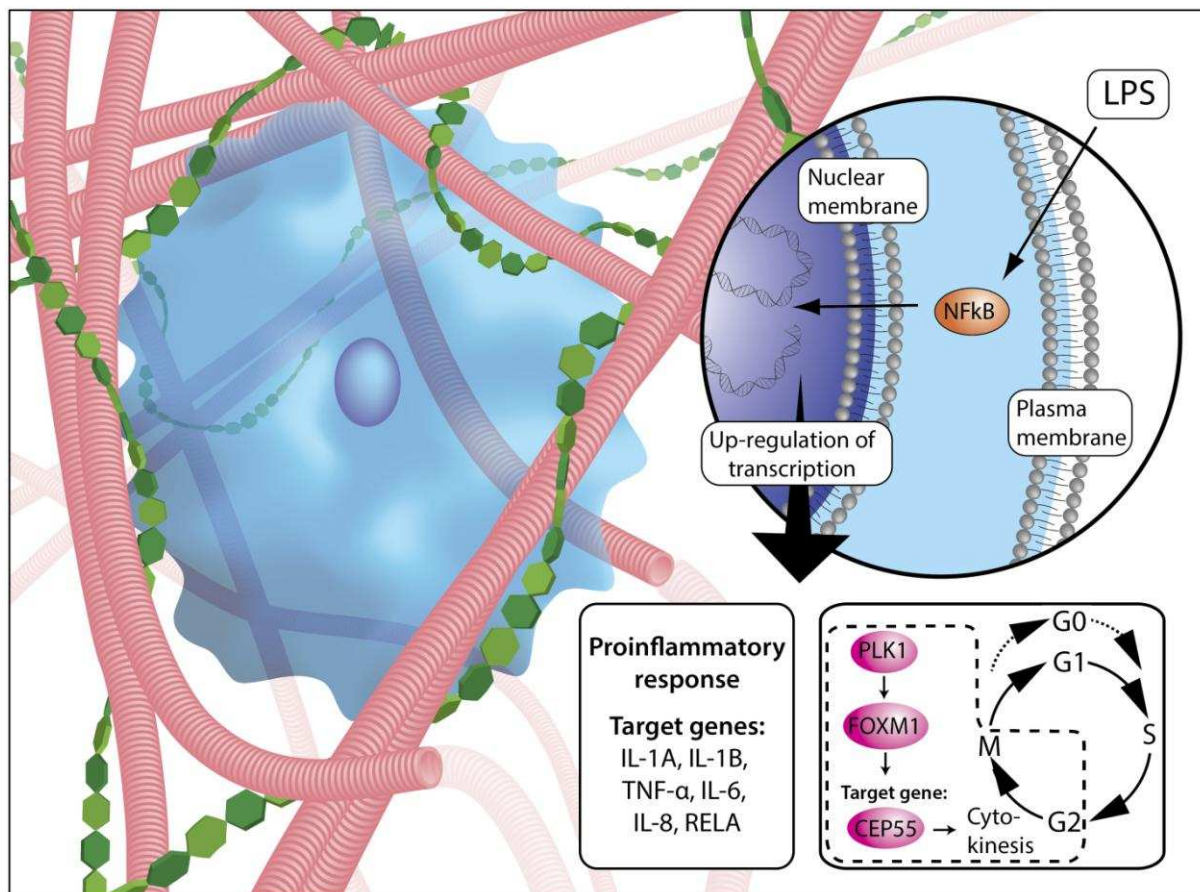


**Figure 5. Co-assembled hydrogels inhibits the expression of proinflammatory cytokines and disrupts cell division on a gene and protein level.** A) Visualisation of protein expression of fluorescent NFκβ p65 and CEP55 immunofluorescence analysis (green) in SCC25 cells localised with a nuclear counterstain of Hoechst dye (blue) cultured on the hydrogels for 48 h B) shows NFκβ p65 in the nucleus increasing with 10 μg/mL of LPS stimulation in 0RGD cultures, whereas CEP55 expression was high in SCC25 cells irrespective of stimulation with LPS. Both signals were significantly reduced in cells cultured on the 2RGD hydrogels. Scale bars 25μm. C) Gene expression profiles of the pro-inflammatory cytokine response elements in LPS stimulated and non-stimulated SCC25 cells as determined by qPCR. Interestingly, in each case, gene expression was reduced on the 2RGD hydrogels compared with 0RGD. When LPS was used to stimulate the pro-inflammatory pathway, the expression increased significantly on 0RGD in each case, but remained comparable to the unchallenged cells on 2RGD. \* p = 0.05, \*\* p = 0.01, \*\*\* p = 0.001 \*\*\*\* p = 0.0001



### Graphical abstract

The self-assembly of a peptide and a polysaccharide results in a nanostructured multifunctional scaffold that presents high density epitopes for healthy cell culture, whilst creating an anti-inflammatory environment to interrupt the cell cycle and induce apoptosis in cancer cells.